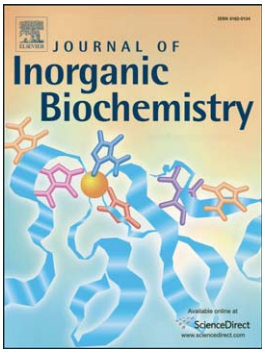

Novel mixed metal Ag(I)-Sb(III)-metallotherapeutics of the NSAIDs, aspirin and salicylic acid. Enhancement of their solubility and bioactivity by using the surfactant CTAB

E.I. Gkaniatsou, C.N. Banti, N. Kourkoumelis, S. Skoulika, M. Manoli, A.J. Tasiopoulos, S.K. Hadjikakou

PII: S0162-0134(15)00108-7
DOI: doi: 10.1016/j.jinorgbio.2015.04.014
Reference: JIB 9714

To appear in: *Journal of Inorganic Biochemistry*

Received date: 9 February 2015
Revised date: 17 April 2015
Accepted date: 17 April 2015

Please cite this article as: E.I. Gkaniatsou, C.N. Banti, N. Kourkoumelis, S. Skoulika, M. Manoli, A.J. Tasiopoulos, S.K. Hadjikakou, Novel mixed metal Ag(I)-Sb(III)-metallotherapeutics of the NSAIDs, aspirin and salicylic acid. Enhancement of their solubility and bioactivity by using the surfactant CTAB, *Journal of Inorganic Biochemistry* (2015), doi: 10.1016/j.jinorgbio.2015.04.014

Novel mixed metal Ag(I)-Sb(III)-metallotherapeutics of the NSAIDs, aspirin and salicylic acid. Enhancement of their solubility and bioactivity by using the surfactant CTAB.

E.I. Gkaniatsou[a], C.N. Banti[a], N. Kourkoumelis*[b], S. Skoulika[c], M. Manoli[d], A.J. Tasiopoulos[d] and S.K. Hadjikakou*[a].

[a] Inorganic and Analytical Chemistry, Department of Chemistry, University of Ioannina, 45110 Ioannina, Greece.

[b] Medical Physics Laboratory, Medical School, University of Ioannina, 45110, Ioannina, Greece.

[c] Section of Physical Chemistry, Department of Chemistry, University of Ioannina, Ioannina, Greece

[d] Department of Chemistry, University of Cyprus, 1678, Nicosia, Cyprus

*All correspondence should be addressed to:

* Dr N. Kourkoumelis (Assistant Professor): e-mail: nkourkou@uoi.gr; Tel xx30-26510-07594

* Dr S.K. Hadjikakou (Professor); e-mail: shadjika@uoi.gr; tel. xx30-26510-08374

fax xx30-26510-08786

Abstract

The already known Ag(I)-Sb(III) compound of the formula {$Ag(Ph_3Sb)_3(NO_3)$} (**1**) and two novel mixed metal Ag(I)-Sb(III) metallotherapeutics of the formulae {$Ag(Ph_3Sb)_3(SalH)$}(**2**) and {$Ag(Ph_3Sb)_3(Asp)$}(**3**) ($SalH_2$= salicylic acid, AspH = aspirin or 2-acetylsalicylic acid and Ph_3Sb= triphenyl antimony(III)) have been synthesised and characterised by m.p., vibrational spectroscopy (mid-FT-IR), ^{13}C-,^{1}H-NMR, UV-visible (UV-vis) spectroscopic techniques, high resolution mass spectroscopy (HRMS) and X-ray crystallography. Compounds **1**,**-3** were treated with the surfactant cetyltrimethylammonium bromide (CTAB) in order to enhance their solubility and as a consequence their bioactivity. The resulting micelles **a-c** were characterised with X-ray powder diffraction (XRPD) analysis, X-ray fluorescence (XRF) spectroscopy, Energy-dispersive X-ray spectroscopy (EDX), conductivity, Thermal gravimetry–differential thermal analysis (TG–DTA), and atomic absorption. Compounds **1**-**3** and the relevant micelles **a**-**c** were evaluated for their *in vitro* cytotoxic activity against human cancer cell lines: MCF-7 (breast, estrogen receptor (ER) positive), MDA-MB-231 (breast, ER negative) and MRC-5 (normal human fetal lung fibroblast cells) with sulforhodamine B (SRB) colorimetric assay. The results show significant increase in the activity of micelles compared to that of the initial compounds. Moreover, micelles exhibited lower activity against normal cells than tumor cells. The binding affinity of **a-c** towards the calf thymus (CT)-DNA, lipoxygenase (LOX) and glutathione (GSH) was studied by the fluorescent emission light and UV-vis spectroscopy.

Keywords:

Bioinorganic Chemistry; silver(I)-antimony(III) compounds; anti-inflammatory drugs; micelles; cytotoxic activity**.**

1. Introduction

Metal-based drugs play a crucial role in medicine [1-2]. Compounds with antimony (anti-protozoal), bismuth (anti-ulcer), gold (anti-arthritic), iron (anti-malaria), silver (anti-microbial) and platinum (anti-cancer) are typical examples of metal-based drugs for the treatment of various diseases [1-7]. Despite the widespread use of these metallotherapeutics, the developed cell resistance, their side effects and their low solubility prompt the research towards designing new and safe drugs [8-9]. Moreover, research is focused on limiting the toxicity while enhancing the reactivity.

Silver ions have been extensively used for a variety of medical purposes [10-16]. Silver sulphadiazine is an example of silver containing drug [10]. The anti-bacterial activity of silver compounds has been attributed to its ionized form Ag(I), which interact with thiol-containing proteins and DNA causing cell damage [10,14,17]. This interaction of silver compounds with proteins and DNA combined with their very low toxicity to humans, create a new era for the development of anti-cancer metallotherapeutics [10]. Recent studies have shown selectivity of silver compounds with carboxylic acids towards adenocarcinoma cells [10].

Antimonials (such as potassium antimony tartrate or the less toxic pentavalent, sodium stibogluconate (pentostam) and melglumine antimoniate (glucantime)) have been used for the treatment of leismaniasis (tropical disease) [18-23]. The potential anti-cancer activity of antimony compounds is also under consideration [18-23]. Antimony(III) complexes are more active, mainly, against carcinoma, but less active against lymphoma [18]. It is also notable, that antimony(III) complexes exhibit strong anti-proliferative activity against human cancer cells, which is not observed against murine cells [18]. Specifically, the antimony(III) complexes exhibit selectivity against sarcoma and carcinoma cells [18].

Aspirin (AspH) (Figure 1) and its active metabolite, salicylic acid (SalH2) (Figure 1) belong to the class of non-steroidal anti-inflammatory drugs (NSAIDs). A number of studies relate the use of NSAIDs with a reduction in the incidence of colorectal, bladder, prostate, lung cancer and breast

cancer, identifying them as selective anticancer agents [24-28]. NSAIDs also target lipoxygenase (LOX). LOX is a class of enzymes responsible for the conversion of arachidonic, linoleic and other polyunsaturated fatty acids into biologically active metabolites [29]. LOX is mainly distributed to the mitochondrion [15]. Studies on the relationship between NSAID-induced apoptosis and the inhibition of lipoxygenase, concluded that LOX is an additional molecular target [11-16,30-32].

Micelles, on the other hand, can be used as drug carriers with the added benefit of increasing the bioavailability of the drug allowing them to accumulate in areas with tumours [33-35]. The solubility can be improved using surfactants like the cationic cetyltrimethylammonium bromide (CTAB) (Figure 1) [36]. CTAB has been widely used in the preparation of gold nanoparticles [37-38] and in several studies concerning the encapsulation of poorly soluble drugs in water [39]. Its low toxicity in clinical trials [40] and its potential anticancer activity [41] have been the key factors in our study.

Since DNA is targeted, by current chemotherapeutics of cancers [11-16] the development of new DNA binders that intercalate into either minor of major grooves is a critical aspect for the development of new drugs. Moreover, glutathione (GSH), plays an important role in multi-drug resistance since GSH readily interacts with chemotherapeutics preventing substantial quantities of them from reaching DNA in the nucleus and ultimately limit their efficacy [12]. High levels of GSH ave been found in many tumours including breast cancer that show different degrees of multidrug resistance, including breast cancer [12].

Breast cancer is hormone dependent malignancy [12]. Since estrogen receptors (ERs) are expressed in human breast cancer, they probably act as both a growth and a survival factors for breast cancer [12]. MCF-7 (breast, ER positive) and MDA-MB-231 (breast, ER negative) are two human breast cancer cell lines where the ERs are devoid (MDA-MB-231), or present (MCF-7) [12].

Our studies aim at the development of new metallotherapeutics [11-16,18-23] which overcome the cell resistance while they can interact with ERs causing a selective inhibition of breast cancer cells. In the course of these studies we have synthesize silver(I) complex

{$Ag(Ph_3Sb)_3(NO_3)$} (**1**) (Ph_3Sb= triphenyl antimony) (Figure 1)) [42], was used as a precursor for the synthesis of {$Ag(Ph_3Sb)_3(SalH)$}(**2**). The complex {$Ag(Ph_3Sb)_3(Asp)$}(**3**) is also prepared. The compounds **1-3** were characterised by m.p., FT-IR, ^{1}H-,^{13}C-NMR, UV-vis spectroscopic techniques, HRMS and single crystal X-ray diffraction analysis. The stability of the complexes in DMSO solution has been verified by means of ^{1}H- NMR, UV-vis and conductivity measurements. The micelles **a-c** was characterized by atomic absorption, conductivity, Thermal gravimetry–differential thermal analysis (TG–DTA) (TG–DTA), X-ray powder diffraction (XRPD) analysis, X-ray fluorescence (XRF) spectroscopy and Energy-dispersive X-ray spectroscopy (EDX). The *in vitro* cytotoxic activity of the compounds **1-3** and their micelles **a-c** against MCF-7 (breast, ER positive), MDA-MB-231 (breast, ER negative) and MRC-5 (normal human fetal lung fibroblast cells) was evaluated and the results are discussed in comparison. The binding affinities of micelles **a-c** towards the intracellular molecules of calf thymus (CT)-DNA, glutathione (GSH) and lipoxygenase (LOX) were studied by fluorescence and UV-vis spectroscopies.

Figure 1

2. Results and discussion

2.1. General aspects: Compound **1** was synthesised through the reaction of $AgNO_3$ with Ph_3Sb (Diagram 1). Crystals of **1** (Figure S1) (1st preparation: $P2_1/n$, a= 17.815(2), b= 14.488(2), c= 19.648(4) Å, β= 97.130(10)^{o}; 2nd preparation: $P2_1/n$, a= 17.3575(7), b= 14.4695(5), c= 19.4437(9) Å, β= 96.051(4)^{o}) are similar to the known one ($P2_1/n$: a= 19.602(5), b= 14.455(1), c= 17.727(2), β= 97.19(2)^{o}) [42]. However, the small variations in the unit cell parameters (β angle) led us to refine the structure again. Complex **1** was then used as a precursor for the formation of compound **2.**

The reaction of **1** with salicylic acid in the presence of an excess of $(CH_2CH_3)_3N$ in CH_3OH/CH_3CN solution yielded the compound **2** (Diagram 1). X-Ray Powder Diffraction (XRPD)

analysis was performed in order to compare the two products. Compound **2** was also prepared by the reaction of $SalH_2$ with $AgNO_3$, followed by the addition of Ph_3Sb in DMSO solution (Diagram 1). The diffraction patterns in XRPD indicate that the two products of **2** obtained from these two reactions are identical. (Figure S2). Moreover the intermediate complex silver salicylate, [Ag(Sal)] (Figure S3) was isolated during this procedure as an intermediate: space group $P2_1/c$; monoclinic; a= 7.4100(10), b= 8.8350(10) and c= 10.687(2) Å; β= 107.630(10)^o;V= 666.79(17) Å^3 Z= 4, T= 293(2) K, D(calc)= 2.4404(7) g cm^{-3}; μ= 2.964 mm^{-1} which is identical to the known one ($P2_1/c$, a= 7.405(1), b= 8.826(2), c= 10.Å, β = 107.48(4)^o) [16,43].

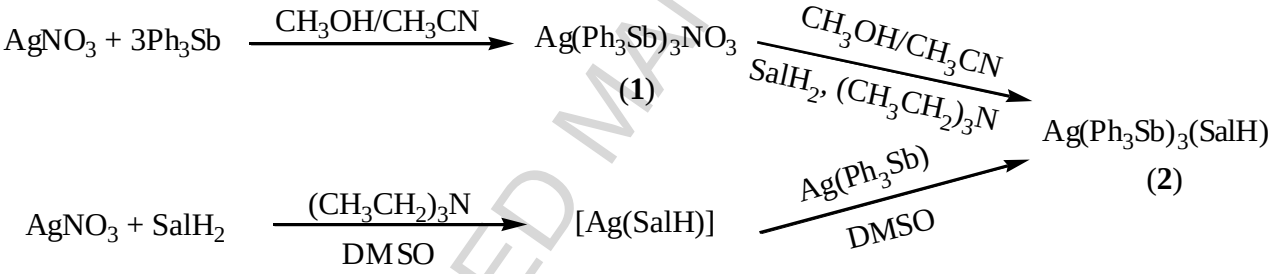

Diagram 1

Compound **3** was synthesised with an alternative method to overcome the hydrolysis of aspH which occurs when **1** reacts with aspH directly (Diagram 2, procedure **I**). The esterification reaction of the salicylic acid of **2** was attempted (Diagram 2, procedure **II**). Compound **2** was treated with acetic anhydride in the presence of small amounts of the catalyst, phosphoric acid. However, the new product obtained was the diacetic-triphenyl antimony, [$Ph_3Sb(Ac)_2$]. The product was characterised by single crystal X-ray diffraction (Figure 2). Compound **3** was finally obtained by the reaction of aspirin with $AgNO_3$ in the presence of excess of $(CH_2CH_3)_3N$ [44], followed by the addition of Ph_3Sb in DMSO solution (Diagram 2, procedure **III**).

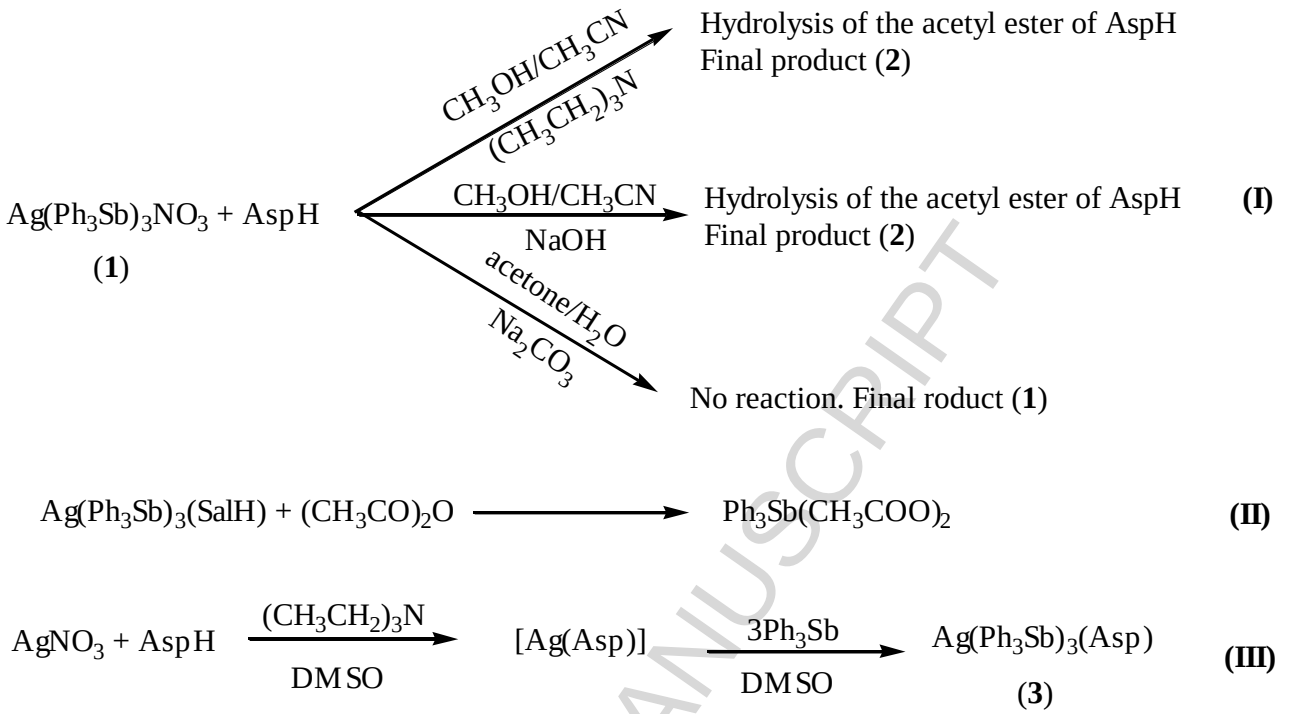

Diagram 2

Figure 2

Crystals of the compounds **1** and **2** have been formed through slow evaporation of CH_3OH/CH_3CN solutions, whereas crystals of the complex **3** have been grown in CH_2Cl_2/toluene solution. The formulae of the compounds were initially examined with spectroscopic methods and their structures were confirmed by single crystal X-ray diffraction analysis. Compound **1** and **2** were soluble in CH_3OH, CH_3CN $CHCl_3$, CH_2Cl_2, $(CH3)_2CO$, DMSO and DMF, while compound **3** was poorly soluble in the above solvents. Micelles **a-c** were formed by adding drop wise aqueous solution of CTAB to a methanolic-aqueous solution (1:3) of the corresponding compound **1-3** (Scheme 1)

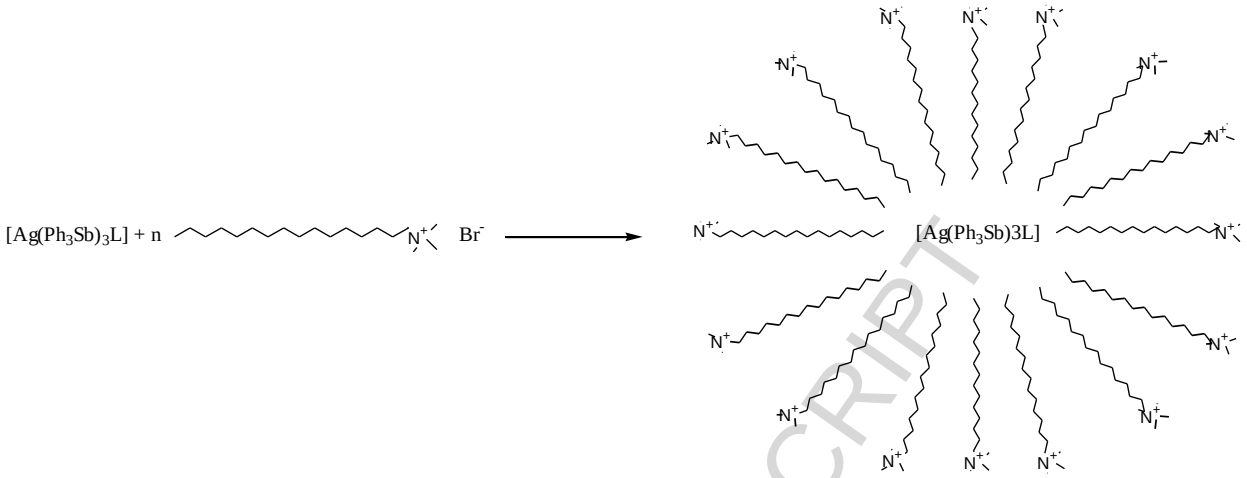

Scheme 1

*2.2 Characterisation Studies of compounds **1**, **2** and **3**:*

2.2.1. Solid state studies:

*Crystal and molecular structure of {Ag(Ph$_3$Sb)$_3$(NO$_3$)} (**1**), {Ag(Ph$_3$Sb)$_3$(SalH)}(**2**) and {Ag(Ph$_3$Sb)$_3$(Asp)}(**3**):* The structure of compound **1** (Figure S1) is known [42], (**1**: crystallized in *P*2$_1$/*n*, *a*= 17.815(2), *b*= 14.488(2), *c*= 19.648(4) Å, *β*= 97.130(10)^o; **NOPQUE**: *P*2$_1$/*n*, *a*= 19.602(5), *b*= 14.455(1), *c*= 17.727(2) Å, *β*= 97.19(2) ^{o}, [42]) (Figure S1). ORTEP diagram of **2**-**3** are shown in Figures 3-4.

Figures 3-4

In the case of **2** and **3**, three antimony atoms from Ph_3Sb and one oxygen atom from the deprotonated carboxylic group of salicylic acid and aspirin respectively, form a tetrahedral geometry around Ag(I) ion. The average Ag-Sb bond distance in **2** is 2.737 Å (Ag-Sb1= 2.716, Ag-Sb2= 2.695 and Ag-Sb3= 2.799) and in **3** is 2.727 Å (Ag-Sb1= 2.7233(8), Ag-Sb2= 2.7393(7) and Ag-Sb3= 2.7179(7)). The Ag–O bond distance in **2** is 2.297 Å and in **3** is 2.391(6) Å, while the corresponding bond distances observed in silver(I) mixed ligand complexes of triphenylphospine with salicylic acid or aspirin were 2.4045(12) Å and 2.5230(12) Å, respectively [16].

Vibrational spectroscopy: The spectrum of compound **1** shows vibrational bands at (i) 1406 cm^{-1} which is assigned to ν_{as} (NO_2), (ii) 1384 cm^{-1} of the ν_s (NO_2) and (iii) 1036 cm^{-1} for the ν(NO) vibration. The Ph-Sb frequency is near 450 cm^{-1}, but it is hidden by the strong phenyl band at 454 cm^{-1} (Figure S4). The IR spectrum of the complex **2** shows a vibrational band at 3443 cm^{-1}, which is assigned to ν(phenolic OH) [45]. The corresponding vibrational band ν(O-H) of the free ligand appears at 3340 cm^{-1}. The $\nu_{as}(COO^-)$ vibration of the free ligand appears at 1659 cm^{-1} and the $\nu_s(COO^-)$ at 1325 cm^{-1}. The corresponding $\nu_{as}(COO^-)$ vibration on **2** is observed at 1589 cm^{-1} and the $\nu_s(COO^-)$ at 1254cm^{-1} (Figure S5). For compound **3**, the vibrational band at 1769 cm^{-1} corresponds to ν(C=O) of the ester group whereas the ν(C=O) of the carboxylic group appears at 1743 cm^{-1} [16]. The respective vibrational bands in the free ligand are found at 1753 cm^{-1} and 1694 cm^{-1}. The ν(C-O) vibration can been seen at 1221 cm^{-1} and 1217 cm^{-1} in the free ligand and **3** respectively [16] (Figure S6).

2.2.2. Solution studies:

^{1}H-NMR studies: Compound **1** has three different types of protons 2-ortho (H^a), 2-meta (H^b) and 1-para (H^c) in each phenyl group of Ph_3Sb (Figure S7, Figure 1). The resonance signals of these protons appear as a multiple peak in the ^{1}H-NMR spectrum at 7.51-7.42 ppm in DMSO-d_6 solution. In compound **2**, the aromatic protons of the Ph_3Sb groups appear as a multiple at 7.51-7.42 ppm (Figure S8, Figure 1). The hydroxyl proton, H^h of compound **2** does not appear in the range of 9-10 ppm, where it is expected [45], suggesting fast exchange with DMSO-d_6 (Figure 1). The doublet signal at 7.77-7.74 ppm is attributed to the proton H^d of the phenyl group, as it is closer to the carboxyl group (i.e. less shielded). The triplet signal at 7.23-7.17 ppm is assigned to the H^f proton, whereas H^e, H^g appears as a multiplet at 6.71-6.64 ppm. The respective signals of the free ligand ($SalH_2$) are observed at 11.5 ppm (s, H^h), 7.81-7.78 ppm (d, H^d), 7.48-7.45 ppm (t, H^f), 6.94-6.25 ppm (d, H^g) and 6.91-6.68 ppm (t, H^e) [15-16]. Compound **3**, shows a singlet at 2.58 ppm that corresponds to the methyl protons H^h of the ligand Asp [15-16] (Figure S9a). The doublet signal at

7.93-7.90ppm is attributed to the less shielded proton H^d. The triplet at 7.28-7.22 ppm corresponds to the proton H^e and the doublet at 7.05-7.02 ppm to the proton H^g. The signal of the proton H^f which is expected to be observed at ~7.4 ppm and it is overlapped with the multiplet signal of the the Ph_3Sb protons (~7.48 ppm) (Figure S9b). The respective signals of the free ligand (AspH) are observed at 2.30 ppm (s, H^h), 8.05 ppm(d, H^d), 7.36 ppm (t, H^e), 7.15 ppm (d, H^g), whereas the triplet of H^f, appears at 7.62 ppm [15-16].

Stability studies: The stability of **1-3** was tested by UV-vis, and ^{1}H-NMR spectroscopy for a period of 1 week in DMSO-d_6 solutions. No changes were observed between the initial UV spectrum and the corresponding spectra of **1-3** measured after 24, 48 hrs and 1 week for all three compounds indicating no disintegration. (Figure S10). There was no change observed in the ^{1}H-NMR spectra of compound **1-3** (Figure S11-S13).

*2.3. Characterisation Studies of micelles **a**, **b** and **c**:*

2.3.1. Solid state studies:

*X-ray fluorescence spectroscopy: S*emi-quantitative XRF analysis has been used in order to assert the encapsulation of compounds **1-3** in the micelles' structures **a-c** respectively (Figure 5). The results testify the presence of the compounds in the final structures. The ratios of Sb:Ag were determined from the integration of the peaks, Ag K_α (22.1 keV) and Sb K_α (26.3 keV) and the sensitivity curve of the device, in the region of 11-40 keV. The peaks of indium derive from the shielding material of the source. The presence of Ag and Sb was initially confirmed by EDX measurements. However, reliable elemental quantification was not achieved due to the low concentration of each element and the inhomogeneous nature of the samples [46]. A typical electron microscopy (SEM) image (micelle **b)** accompanied by qualitative EDX analysis for complex **2**, are shown in Figure S14.

Figure 5

Thermal analysis: The weight loss of **a-c** was monitored while the temperature increased at a rate of 10°C min^{-1} from ambient up to 600°C, under nitrogen-air flow (Figure S15). TG/DTA analysis shows an endothermic peak between 200-280 (**a**) 210-290 (**b**) and 200-300 (**c**) ^{o}C, which is attributed to the loss of all ligands and surfactant molecules. The 10% (**a**), 4% (**b**) and 5% (**c**) TG residues consist of Ag^{0}/Sb_2O_3 mixture. While silver oxide forms as the compounds start to decompose, the oxide melts at 280^{o}C and finally elemental silver is formed [47]. On the other hand, Sb_2O_3 that is produced from the Ph_3Sb groups remains stable up to 653^{o}C [48].

2.3.2. Solution studies:

Atomic Absorption: The mass of the silver contained in each micelle was measured via graphite furnace atomic absorption (GFAAS). The percentage (%) of the compound engulfed in the micellar structure is concluded by the amount of silver detected (Table 1). The percentage of the compounds **1-3** in the micelle **a-c** are 0.66(**1**), 0.60(**2**) and 1.76(**3**) %.

Table 1

Conductivity measurements for critical micelle concentration (CMC) determination: In order to assert the formation of micelles the determination of the CMC via the conventional conductivity method [49] at 303 K was performed. The results were compared with the corresponding CMC of pure CTAB and those found in the presence of the co-solvents (CH_3OH/CH_3CN). Below the CMC the solubility of hydrophobic substances is enhanced by providing regions of interaction with the solvent (vesicular cavities). Above the CMC, surfactant molecules self-aggregate to form micelles.

A break-point is observed in the values of conductivity of the micellar solution with the formation of the micelles (Figure 6). The changes on the CMC in the presence of the compounds **1-3** were studied -in the same volumes of the co-solvents- and found to be 1.40 x 10^{-3}, 2.0 x 10^{-3} and 2.0 x 10^{-3} mol dm^{-3} respectively (Figure 6). By taking into account the concentration of the complexes used (2.5 x 10^{-5} mol dm^{-3}) the CTAB complex ratio is 56 (**1**), 80 (**2-3**). The formation of the micelles has been confirmed by the concentrations that had been used for their preparation which were much greater than the found CMCs. The CMC of pure CTAB in water was determined and it agrees with the values reported (~ 1.25 x 10^{-3} mol dm^{-3}) [49]. The effect of the co-solvents used for the dissolution of the compounds was investigated (CH_3OH and CH_3CN 3 mL, ratio 1:1) on CMC. A twofold increase of the CMC (~ 2.50 x 10^{-3} mol dm^{-3}) was observed.

Figure 6

2.4. Biological Tests – Cytotoxicity: Complexes **1**-**3** and micelles **a**-**c** were tested for their *in vitro* cytotoxic activity against MCF-7 (breast, ER positive), MDA-MB-231 (breast, ER negative) and MRC-5 (normal human fetal lung fibroblast cells). MCF-7 and MDA-MB-231 are two human breast cancer cell lines where the ERs are absent (MDA-MB-231), or present (MCF-7) [12] MRC-5 cells (normal human fetal lung fibroblast cells) are used to evaluate the toxicity of the compounds. The IC_{50} values (50 % of cell viability) are summarized in Table 2. Cell survival was estimated by means of SRB assay after 48 hrs of incubation. The results reveal that MCF-7 cells are more

sensitive to compounds **1-3** with IC_{50} values 3.05 (**1**), 3.19 (**2**) and 5.88 (**3**) μM, than MDA-MB-231 cells IC_{50} values 5.67 (**1**), 7.26 (**2**) and 14.86 (**3**) μM) indicating involvement of estrogen receptors in their mechanism of action. The compounds (**1-3**) were toxic on normal cells (4.36 (**1**), 5.03 (**2**) and 4.75 (**3**) μM). The activities of **2** and **3** against MCF-7 and MRC-5 are lower than the corresponding ones $[Ag(tpp)_2(SalH)]$, $\{[Ag(tpp)_3(asp)](dmf)\}$, $[Ag(tptp)_2(salH)]$ and $[Ag(tmtp)_2(salH)]$ [11,16] (Table 2) where instead of triphenylstibine, the ligand is triphenylphospine, tri(*p*-tolyl)phosphine (tptp) or tri(*m*-tolyl)phosphine (tmtp).

Table 2

The encapsulation of the compounds **1-3** in the micelles **a-c**, results in a boost of their cytotoxic activity (Table 2). Micelles show 67.8-fold (**a**) 66.5-fold (**b**) and 57.1-fold (**c**), increased activity against MCF-7 and 135-fold (**a**) 165-fold (**b**) and 57.1-fold (**c**), against MDA-MB-231. Moreover, MRC-5 cells are more resistant to the micelles' action, when compared in the cancer cells lines. The therapeutic potency index (TPI) [12] of the tested compounds, which is defined as the IC_{50} value against normal cell lines divided by the IC_{50} value against cancer cell lines of the same or similar tissue are also determined. The higher the TPI value is, the better the potency of the metallotherapeutic agent. Although, the complexes exhibit high toxicity, their micelles are not toxic indicating better therapeutic index (Table 2). Finally, the encapsulated complexes **1-3**, into micelles **a-c,** exhibit higher selectivity to tumor cells than normal.

The mechanisms of action of **a-c** were further investigated by the DNA binding studies, LOX inhibitory activity and their interaction with GSH.

2.5. DNA binding studies:

*2.5.1. UV-absorption spectral studies***:**

The interaction of the micelles with CT-DNA has been investigated by UV absorption spectroscopy. There are three modes of DNA binding (a) Electrostatic interaction with the negatively charged nucleic sugar-phosphate structure, which are along the external DNA double helix and do not possess selectivity (b) binding interaction with two grooves of DNA double helix and (iii) intercalation between the stacked base pairs of native DNA [50]. Especially, the intercalation can be clarified by the hypochromism as a result of the disconfirmation of DNA in the helix axis. A slight decrease in the absorption intensity (at λmax= 261 nm) is observed upon the presence and absence of **a-c** at various r values (r= [complex]/[DNA], [DNA]= $5x10^{-5}$ M) which is attributed to the intercalation binding between DNA and micelles **a-c** (Figure S16).

The binding constants (*Kb*) of micelles **a-c** towards CT-DNA were evaluated by monitoring the changes in the absorbance of the UV spectra ([a]= 3.9 mM, [b]= 3.0 mM, [c]= 5.0 mM), at 300-310 nm, with increasing concentration of CT-DNA (Figure S17). K_b is obtained as previously reported in the Ref's [11-16]. The calculated K_b values for **a-c** are: (3.3±0.1)× 10^4 (**a**), (10.0±0.1) ×10^4 (**b**) and (2.5±0.1) ×10^4 (**c**) M^{-1} respectively, suggesting interaction with CT-DNA (Table 3)

Table 3

2.5.2. Fluorescence spectroscopic studies: Fluorescence spectroscopy is an effective method to study metal complexes DNA interaction [11]. Ethidium bromide (EB) emits in the presence of DNA due to its strong intercalation between the adjacent DNA base pairs [11]. The displacement of EB (quantified by fluorescence) by the titration of a compound is suggestive of an intercalative binding [11]. The emission spectra at 610 nm of the EB (2.3 μM) solutions which contain CT-DNA (26 μM) in the absence or presence of various concentrations of micelles **a-c** (0-5.4 μM) were recorded upon their excitation at 527 nm (Figure 7). The apparent binding constant (K_{app}) was calculated as described earlier [11]. Their K_{app} values are 2239±178×10^4 (**a**), 2262±134×10^4 (**b**) and 1129±251×10^4 (**c**) M^{-1} suggesting an intercalative or minor groove binding of both complexes

(Table 3). The high cytotoxic activity of the micelles might be attributed to the significant high K_{app} values which is due to their intercalating interaction with DNA.

Figure 7

*2.6. Study of the peroxidation of linoleic acid by the enzyme lipoxygenase in the presence of micelles **a-c**:* LOX inhibition is known to induce apoptosis [11-16] so the influence of micelles **a-c** on the oxidation of linoleic acid by the enzyme LOX was studied in a wide concentration range (Figure S18). The degree of LOX activity (A, %) in the presence of these compounds was calculated according to the method described previously [11-16]. The **a** shows high inhibitory activity with IC_{50} value of 8.4 μM in contract to the lower activity exhibited by **b** (IC_{50}= 29.4 μM) (Table 3). However, no IC_{50} value was determined for **c**, at the concentrations tested (IC_{50} >30 μM) (Table 3).

*2.7. Reaction of micelles **a-c** with GSH as Monitored by UV Absorption*: As the deactivation of cisplatin, caused by glutathione seems to be an important determinant of its cytotoxic effects, the reaction of micelles **a-c** with GSH was investigated. The initial UV spectra of the solutions (final volume of 2.0 mL) containing different concentrations of **a-c** (68 (A), 140 (B) and 250 (C) μM (**a**); 150(A), 310 (B) and 580 (C) μM (**b**); 360 (A), 730 (B) and 1360 (C) μM (**c**)) in 100 mM Tris-HCl, pH= 7.4 with a high excess of GSH (16.5 mM) at 37° C and after 1, 2, 3, 4 and 5 hrs are shown in Figures S19-21. The increasing absorption intensity of the solution with time is partially due to the reaction of metal complex with GSH (formation of metal-sulphur bonds) and partially due to the oxidation of GSH (formation of the disulfide GSSG), as evidence by the increased absorption with time for GSH alone [12]. However, as the rate of disulfide formation is low, the concentration of GSH was assumed not to change much over the time course due to the GSH-complex reaction. Because the GSH concentration is higher than that of **a-c**, the reaction of GSH with the complexes

does not deplete GSH [12]. The absorbance associated with GSH-complex formation is obtained, by subtracting the absorbance due to the disulfide from the observed absorbance (Figures S22-S24). The absorbance at 280 nm is mainly due to the formation of Ag-GSH products [12].

The initial rate of the reaction between GSH and a metallotherapeutic agent is calculated as described previously [12]. The difference curve is fitted to the equation: $I_d = C + A_1 \exp(-b_1 t) + A_2 \exp(-b_2 t)$ and the initial reaction slope (So) is then derived from the equation $So = -(A_1 b_1 + A_2 b_2)$ [12]. Table 4 summarizes the results for **b-c** whereas micelle **a** does not interact with GSH. The order of the reaction towards a metallotherapeutic agent is calculated by the equation $So_i = k\,[complex]_i^x$ and alternatively from the ln(So) *vs.* ln([complex]) graph (Table 4). The x value shows that the reaction is of first order towards complex **b-c**.

Table 4

3. Conclusions

The new silver(I)-antimony compounds of the anti-inflammatory drugs salicylic acid and aspirin **2-3** have been synthesized and fully characterized. Compounds **1-3** were poorly soluble in most solvents (including H_2O) and therefore were treated with the surfactant CTAB to enhance their properties (solubility and bioavailability).

The compounds and their micelles were tested for their *in vitro* cytotoxicity against the cancer cell line MCF-7 (positive to ER) and MDA-MB-231 (negative to ER) and the normal cell line MRC-5. MCF-7 (positive to ER) cells are more sensitive to **1-3** than MDA-MB-231 (negative to ER) indicating involvement of estrogen receptors in their mechanism of action. Compounds, **1** and **2** showed the better cytotoxic activity against cancerous cells. The activities of **2** and **3** against cells are lower than the corresponding silver(I) compounds where the ligand is tpp, tptp or tmtp instead of Ph_3Sb (Table 2) demonstrating the role of the ligand type. Micelles **a-c**, exhibit improved cytotoxicity ranging from 67.8 to 135 times higher than the initial compounds against MCF-7 and

MDA-MB-231 which is attributed to the better solubility of the compounds. The encapsulated complexes **1-3**, into micelles **a-c,** exhibit higher selectivity to tumor cells than normal which is also observed in the initial compounds **1-3** (Table 2). Thus, the encapsulated compounds **1-3** retained their selectivity against tumor cells.

The mechanism of action of the micelles **a-c** was investigated by mean of their DNA binding affinity, their LOX inhibitory activity and their interaction with GSH. The compounds **a-c** strongly intercalates DNA (K_{app} values are in the magnitude of 1000 x 10^4 M^{-1}). The positive charged micelles (due to the CTAB) (Scheme 2) might be attracted by the negative phosphoric groups of DNA backbone, increasing the binding affinity of the compounds towards DNA. Micelles **a** and **b** which contain the nitrate and salycilate compounds **1** and **2** respectively, interact stronger with DNA than micelle of **c** (which contain aspirinate compound **3**). The micelles **a-c** also inhibit LOX (an enzyme which mainly distributed in the mitochondrion [15]) with the same manner as they interact with DNA. Thus micelles **a** and **b** inhibit LOX activity. The higher binding affinity of **1-2** against DNA and their stronger inhibitory activity against LOX towards the corresponding ones of **3,** might be attributed to the ionic nature of compound **1** and to the hydrogen bonding affinity of **2** through the –OH group of $SalH_2$ towards AspH. Recently, cisplatin was found to interact with a number of other possible targets such as RNA, sulfur-containing enzymes (metallothionein and glutathione) and mitochondrion as well [51]. Similarly, to cisplatin compounds **a** and **b** were found to interact with nuclear DNA and maybe with mitochondrion [51].

4. Experimental

4.1. Materials and instruments: All reagents were purchased from commercial sources and used as received. Solvents used were of reagent grade, while salicylic acid, acetylsalicylic acid, triphenylantimony(III), silver(I) nitrate and cetyltrimethylammonium bromide (Sigma-Aldrich, Merck) were used without further purification. MDA-MB-231 cells were purchase from the American Type Culture Collection (ATCC, Rockville, MD, USA) and the Imperial Cancer

Research Fund (ICRF), London. MCF-7 cells are of the most cited breast cell lines, while MRC-5 is the most common control cell line. Melting points were measured in open tubes with a Stuart scientific apparatus and are uncorrected. X-ray powder diffraction patterns were obtained using a Bruker AXS D8 Advance diffractometer in Bragg–Brentano geometry equipped with a Cu sealed-tube radiation source (λ=1.54178 Å) and a secondary beam graphite monochromator. The whole 2θ range was measured in steps of 0.02 with a counting time of 5 s per step. Infra-red spectra in the region of 4000–370 cm^{-1} were obtained in KBr discs, with a Perkin–Elmer Spectrum GX FT-IR spectrophotometer. The ^{1}H- NMR spectra were recorded on a Bruker AC250 MHz FT-NMR instrument in DMSO-d_6 solution. Chemical shifts δ are reported in ppm using ^{1}H TMS as an internal reference. Thermal studies were carried out on a Shimadzu DTG-60 simultaneous DTA-TG apparatus, under air-N_2 flow (50 cm^3 min^{-1}) with a heating rate of 10 ˚C min^{-1}. A Jasco UV/Vis/NIR V570 series spectrophotometer was used to obtain electronic absorption spectra. XRF measurement was carried out using an Am-241 radioisotopic source (exciting radiation 59.5 keV). For the detection of X-ray fluorescence a Si (Li) detector was used. The measuring time was chosen so as to collect ~ 2000 data on the weaker K_α peak. Graphite furnace atomic absorption (GFAAS) was measured in a Shimadzu AA6300 instrument. Conductivity measurements were carried out at 293 K in H_2O-MeOH/MeCN solutions with a WTF LF-91 conductivity meter.

4.2. Synthesis and crystallisation: (**1**): A solution of 0.5 mmol $AgNO_3$ (0.085 g) in CH_3OH/CH_3CN (3 mL, 1:1) was mixed with to a stirred solution of 1.5 mmol Ph_3Sb (0.530 g) in CH_3OH/CH_3CN (7 mL, 1:1). The mixture was stirred for 30min at room temperature and the resulting clear solution was kept in darkness. Colourless crystals of **1** suitable for X-ray analysis were grown from slow evaporation of the solution after 2 days. (**2**): A solution of 0.08 mmol **1** (0.100 g) in CH_3OH/CH_3CN (3 mL, 1:1) was mixed with to a solution of 0.08 mmol $SalH_2$ (0.011 g) in CH_3OH/CH_3CN (3 mL, 1:1). The mixture was treated with 3.5 mmol $(CH_3CH_2)_3N$ (0.5 mL), added dropwise. The resulting solution was stirred for 30 min at room temperature. Colourless crystals of

2 were grown after 24 hrs. (**3**): Compound **3** was prepared with a different method from **2**. A solution of 0.33 mmol $AgNO_3$ (0.056 g) in DMSO (2 mL) was mixed with to a solution of 0.33 mmol AspH (0.059 g) in DMSO (2 mL), followed by the treatment of 3.5 mmol $(CH_3CH_2)_3N$ (0.5 mL), added dropwise. The mixture was left stirring for 30 min at room temperature, before the addition of 1 mmol Ph_3Sb (0.353 g) in DMSO (4 mL). The final solution was left stirring in darkness for 24 hrs. The light purple precipitate was filtered off and left in the dryer for another 24hrs. Finally, the powder was dissolved in 20 mL CH_2Cl_2/toluene (1:1) and left in the fridge for 1 week, when colourless crystals of the product were collected. The powder was compared with the crystal via XRPD and their diffraction peaks indicate that are identical (Figure S25).

The latter procedure was also used for the preparation of **2** with the respective ligand ($SalH_2$) and the yielded powder product found to be identical with the one synthesised before (Figure S2). When the reaction was stopped at the first step, before the addition of the Ph_3Sb solution, we were able to isolate crystals suitable for X-ray of the already know compound of silver salicylate [43]. The same try was also made in the case of **3**, but no crystals were formed from the already know [AgAsp] compound [44].

1: Colourless crystal, Yield: 70%; melting point: 209-212 °C; Elemental analysis found: C: 52.30; H: 3.61, N: 1.48 %; calculated for $C_{54}H_{45}AgNO_3Sb_3$: C: 52.77; H: 3.69; N: 1.14 %. IR (cm^{-1}), (KBr): 3065m, 1576s,1431s, 1406vs, 1384vs, 1259s, 1066s, 996s, 743s 733s, 694vs, 454s; 448s; ^{1}H-NMR (ppm) in DMSO-d_6: 7.51-7.42 ppm (m, H(Caromatic of Ph_3Sb)); UV-vis (DMSO): λ_{max} = 263 nm (logε = 4.64) (Figures S4, S7, S10).

2: Colourless crystal, Yield: 50%; melting point: 167-170 °C; Elemental analysis found: C: 55.96; H: 3.65 %; calculated for $C_{61}H_{50}AgO_3Sb_3$: C: 56.18; H: 3.86 %. IR (cm^{-1}), (KBr): 3443m, 1624s,1589 vs, 1577s, 1478s, 1382s, 1254vs, 1066s, 997s, 731s, 695s 453s; ^{1}H-NMR (ppm) in DMSO-d_6: 7.53- 7.40 ppm (m, H(Caromatic of Ph_3Sb)), 7.72-7.72 ppm (d, (H^d, HSal), 7.69-7.68 ppm (d, (H^g, HSal), 7.21-7.12 ppm (t, (H^e, HSal), 6.68-6.58 ppm (d, (H^f, HSal); UV-vis (DMSO): λmax= 263 nm (logε= 4.59) (Figures S5, S8, S10).

3: Colourless crystal, Yield: 75%; melting point: 184-187 °C; Elemental analysis found: C: 56.44; H: 3.91 %; calculated for $C_{63}H_{52}AgO_4Sb_3$: C: 56.21; H: 3.89 %. IR (cm^{-1}), (KBr): 3045m, 1769vs,1743vs, 1589s, 1558s, 1364s, 1221vs, 1067s, 731s, 695s, 454vs; ^{1}H-NMR (ppm) in DMSO-d_6: 7.53- 7.37 ppm (m, H(Caromatic of Ph_3Sb)), 7.94-7.92 ppm (d, (H^d, HAsp), 7.90-7.89 ppm (d, (H^g, Hasp), 7.28-7.21 ppm (t, (H^e, HAsp), 7.05-7.01 ppm (d, (H^f, HAsp), 2.58 ppm (s, H(-$COOCH_3$, HAsp)),; UV-vis (DMSO): λmax= 263 nm (logε= 4.54) (Figures S6, S9, S10).

*4.3. X-Ray Crystal-Structure Determination of compounds **1**, **2**, **3**, **[Ag(Sal)]$_n$** and **[Ph$_3$Sb(Ac)$_2$]:*

The structures **1**, **2**, **3** and **[Ag(Sal)]** were solved by direct methods and refined by full-matrix least-squares techniques using the SHELXL-97 package. All non-hydrogen atoms have been located by difference Fourier maps and refined anisotropically. All hydrogen atoms except the hydroxyl one (**2**, **[Ag(Sal)]**), have been placed on calculated positions and refined isotropically by using the riding model. The hydroxyl proton has been located by difference Fourier maps and refined isotropically with restrained O-H distance and COH angle. In case of compound **1** the two oxygen atoms of the NO_3^- group were refined over two positions with occupancy factors 0.5.

Intensity data for the crystals of **1** (second time) and **[Ph$_3$Sb(Ac)$_2$]** were collected on an Oxford Diffraction CCD instrument, using graphite monochromated Mo radiation (k = 0.71073 Å). Cell parameters were determined by least-squares refinement of the diffraction data from 25 reflections. All data were corrected for Lorentz-polarization effects and absorption [52-53]. The structures were solved with direct methods with SHELXS 97 [54] and refined by full-matrix least-squares procedures on F 2 with SHELXL 97 [55]. All non-hydrogen atoms were refined anisotropically, hydrogen atoms were located at calculated positions and refined via the ''riding model'' with isotropic thermal parameters fixed at 1.2 (1.3 for CH_3 groups) times the Ueq value of the appropriate carrier atom.

1 (1st preparation): formula, $C_{54}H_{45}AgNO_3Sb_3$: M_r 1229.03; Monoclinic, space group $P2_1/n$, a = 17.815(2), b = 14.488(2), c = 19.648(4) Å, β = 97.13(1)°; Z = 4, V = 5032.0(14) Å^3, $D_{calc.}$ = 1.622 Mg/m^3, MoK_a radiation (0.71073 Å), T = 293(2) K; 9780 reflections collected on a Bruker P4 diffractometer, 8713 unique (Rint=0.0398), 4949 unique reflections with I>2σ(I); For I>2σ(I) R_1 = 0.0660, wR_2 = 0.1771, GOF= 1.036.

1(2nd preparation): formula, $C_{54}H_{45}AgNO_3Sb_3$: M_r 1229.03; Monoclinic, space group $P2_1/n$, a = 17.3575(7), b = 14.4695(5), c = 19.4437(9) Å, β = 96.051(4)°; Z = 4, V = 4856.2(3) Å^3, $D_{calc.}$ = 1.700 Mg/m^3, MoK_a radiation (0.71073 Å), T = 100(2) K; 23480 reflections collected, 8542 unique (Rint= 0.043), 6986 unique reflections with I>2σ(I); For I>2σ(I) R_1 = 0.0459, wR_2 = 0.1699, GOF= 1.07.

2: formula, $C_{61}H_{50}AgO_3Sb_3$: M_r 1304.13; Triclinic, space group P-1, a = 13.288(1), b = 13.920(1), c = 14.943(2) Å, α = 91.69(1)°, β = 90.75(1)°, γ = 102.96(1)°; Z = 2, V = 2691.9(5) Å^3, $D_{calc.}$ = 1.609 Mg/m^3, MoK_a radiation (0.71073 Å), T = 293(2) K; 10716 reflections collected on a Bruker P4 diffractometer, 9395 unique (Rint=0.0238), 7250 unique reflections with I>2σ(I); For I>2σ(I) R_1 = 0.0462, wR_2 = 0.1201, GOF=1.041.

3: formula, $C_{63}H_{52}AgO_4Sb_3$: M_r 1346.17; Triclinic, space group P-1, a = 13.211(2), b = 13.527(1), c = 16.372(2) Å, α = 86.64(1)°, β = 75.82(1)°, γ = 80.95(1)°; Z = 2, V = 2800.7(6) Å^3, $D_{calc.}$ = 1.596 Mg/m^3, MoK_a radiation (0.71073 Å), T = 293(2) K; 11169 reflections collected on a Bruker P4 diffractometer, 9790 unique (Rint=0.0327), 6927 unique reflections with I>2σ(I); For I>2σ(I) R_1 = 0.0426, wR_2 = 0.0940, GOF=1.010.

[Ag(Sal)]: formula, $C_7H_5AgO_3$: M_r 244.98; Monoclinic, space group $P2_1/c$, a = 7.410(1), b = 8.835(1), c = 10.687(2) Å, β = 107.63(1)°; Z = 4, V = 666.79(17) Å^3, $D_{calc.}$ = 2.440 Mg/m^3, MoK_a radiation (0.71073 Å), T = 293(2) K; 1444 reflections collected on a Bruker P4 diffractometer, 1177 unique (Rint=0.0184), 1031 unique reflections with I>2σ(I); For I>2σ(I) R_1 = 0.0268, wR_2 = 0.0670, GOF=1.069.

[$Ph_3Sb(Ac)_2$]: formula, $C_{22}H_{21}O_4Sb$: M_r 471.15; Monoclinic, space group *C2/c*, *a* = 12.7257(9), *b* = 9.8981(7), *c* = 15.6343(12) Å, *β* = 106.972(8)°; Z = 4, V = 1883.5(3) $Å^3$, $D_{calc.}$ = 1.6615(3) Mg/m^3, MoK_a radiation (0.71073 Å), T =100 K; 11169 reflections collected on a Bruker P4 diffractometer, 9790 unique (Rint=0.0327), 6927 unique reflections with I>2σ(I); For I>2σ(I) R_1 = 0.0426, wR_2 = 0.0940, GOF=1.010.

The crystallographic data of the compounds have been deposited with the Cambridge Crystallographic Data Centre as supplementary publication number CCDC-1011503 (**1;** 1st preparation), 1011697(**1**; 2nd preparation), 1011504 (2), 1011505 (**3**), 1011506 (**[Ag(Sal)]**), 1011696 (**[$Ph_3Sb(Ac)_2$]**). Copies of the data can be obtained, free of charge, via the internet (http://www.ccdc.cam.ac.uk/data_request/cif), e-mail (data_request@ccdc.cam.ac.uk), or fax (+44-1223-336033).

4.4. Micellar Synthesis: 0.038 mmol (0.047 g (**1**), 0.049 g (**2**) and 0.051 g (**3**)), were dissolved in CH_3OH/CH_3CN (3 cm^3, 1:1) and stirred at 303 K. 10 cm^3 of distilled H_2O were added to the solution forming a suspension; we would use the low solubility of the compounds in water to identify later the point at which they had been fully engulfed in the micelles. A separate solution of 8 mmol CTAB (3 g) in distilled H_2O (30 cm^3) was prepared, stirred at 303 K and added stepwise (1 cm^3 steps) to the first solution of the respective compound until it became clear, which meant that the majority of the suspended particles were inside the micellar structures. The clear mixture was left stirring for 30 min at 303 K; then it was filtered off and left to evaporate slowly overnight. The micelles were collected as colourless aggregates.

4.5. Cytotoxic activity, DNA binding and LOX inhibitory activity studies: This study was performed as was previously reported [11-16].

5. Table of Abbreviations

AspH	Aspirin
CMC	Crticical Micelle Concentration
CTAB	Cetyltrimethylammonium Bromide
CT-DNA	Calf Thymus DNA
EB	Ethidium Bromide
Er	Estrogen Receptors
GFAAS	Graphite Furnace Atomic Absorption
GSH	Glutathione
GST	Glutathione S-Transferases
K_{app}	Apparent Binding Constant
LOX	Lipoxygenase
MRC-5 cells	Normal Human Fetal Lung Fibroblast Cells
NSAIDs	Non-Steroidal Anti-Inflammatory Drugs
$SalH_2$	Salicylic Acid
So	Initial Reaction Slope
SRB assay	Sulforhodamine B Assay
tmtp	Tri(m-tolyl)phosphine
TPI	Therapeutic Potency Index
tptp	Tri(p-tolyl)phosphine
XRPD	X-Ray Powder Diffraction

Acknowledgements

This work was carried out in partial fulfillment of the requirements for the graduate studies (Master) MSc thesis of Mrs. E.I.G. under the supervision of S.K.H. The National Strategic Reference Framework, Regional Operational Program of Epirus 2007-2013 (2011/S 29-048013), is acknowledged for supporting the purchase of an LS55 fluorimetry instrument to the Department of Chemistry of the University of Ioannina. Dr. C. Papachristodoulou is acknowledged for the XRF measurements. The authors would like to thank the Unit of bioactivity testing of xenobiotics, the University of Ioannina, for providing access to the facilities. CNB and SKH acknowledge the Josef and Esther Gani Foundation for the financial support. CNB and SKH also acknowledge the COST Action CM1105 “Functional metal complexes that bind to biomolecules” for the stimulating discussions. CNB and SKH acknowledge the National Scholarships Foundation of Greece (IKY) for the post doctoral research fellowship of excellence program (IKY)-Siemens.

Appendix A. Supplementary Data

References

[1] S. Medici, M.Peana, V-M. Nurchi, J.I. Lachowicz, G. Crisponi, M-A. Zoroddu, Coord. Chem. Rev. 284 (2015) 329-350

[2] B. Desoize, Anticancer Res, 24 (2004) 1529-1544.

[3] B. Lippert,B. (ed.), Cisplatin. Chemistry and Biochemistry of a Leading Anticancer Drug. Wiley-VCH, Zürich, Switzerland (1999).

[4] N.P. Farrell, L.R. Kelland (eds), Platinum-based Drugs in Cancer Therapy. Humana Press, Totowa, New Jersey, USA (2000)

[5] R. B. Weiss, M. C. Christian, Drugs, 46 (1993) 360-377.

[6] D. Lebwohl, R. Canetta, Eur J Cancer 34 (1998) 1522-1534.

[7] P.J. O'Dwyer, S.W. Johnson, T.C. Hamilton, Cisplatin and Its Analogues, in V.T. DeVita, S. Hellman, S.A. Rosenberg, Cancer: Principles and Practice of Oncology, Ed. 6, 377-388, Lippincott, Williams & Wilkins, Philadelphia, 2001

[8] P.J. O'Dwyer, J.P. Stevenson, S.W. Johnson, Clinical Status of Cisplatin, Carboplatin, and Other Platinum-based Antitumor Drugs, in B. Lippert, Cisplatin: Chemistry and Biochemistry of a Leading Anticancer Drug, 31-72. Wiley- VCH, New York 1999

[9] M.S. Highley, A.H. Calvert, Clinical experience with cisplatin and carboplatin, in L. Kelland, N. Farrel (Eds.), Platinum Based Drugs in Cancer Therapy, Humana Press, Totowa, New Jersey, 2000, pp. 171–194

[10] C.N. Banti, S.K. Hadjikakou, Metallomics, 5, (2013), 569-596.

[11] C.N. Banti, A.D. Giannoulis, N. Kourkournelis, A.M. Owczarzak, M. Kubicki, S.K. Hadjikakou, J Inorg Biochem 142 (2015) 132-144

[12] C.N. Banti, L. Kyros, G.D. Geromichalos, N. Kourkoumelis, M. Kubicki, S.K. Hadjikakou, Eur J Med Chem 77 (2014) 388-39

[13] C.N. Banti, A.D. Giannoulis, N. Kourkoumelis, A.M. Owczarzak, M. Kubicki, S.K. Hadjikakou, Dalton Trans 43 (2014) 6848-6863.

[14] L. Kyros, C.N. Banti, N. Kourkoumelis, M. Kubicki, I. Sainis, S.K. Hadjikakou, J Biol Inorg Chem 19 (2014) 449-464.

[15] C.N. Banti, A.D. Giannoulis, N. Kourkoumelis, A.M. Owczarzak, M. Poyraz, M. Kubicki, K. Charalabopoulos, S.K. Hadjikakou, Metallomics 4 (2012) 545-560.

[16] M. Poyraz, C.N. Banti, N. Kourkoumelis, V. Dokorou, M.J.Manos, M. Simcic, S. Golic-Grdadolnik, T. Mavromoustakos, A.D. Giannoulis, I.I. Verginadis, K. Charalabopoulos, S.K. Hadjikakou, Inorg Chim Acta 375 (2011) 114-121.

[17] Q.L. Feng, J. Wu, G.Q. Chen, F.Z. Cui, T.N. Kim, J.O. Kim, J Biomed Mater Res 52 (2000) 662-668.

[18] I.I. Ozturk, C.N. Banti, M.J. Manos, A.J. Tasiopoulos, N. Kourkoumelis, K. Charalabopoulos, S.K. Hadjikakou, J Inorg Biochem 109 (2012) 57-65

[19] I.I. Ozturk, O.S. Urgut, C.N. Banti, N. Kourkoumelis, A.M. Owczarzak, M. Kubicki, S.K. Hadjikakou, Polyhedron 70 (2014) 172-179

[20] I.I. Ozturk, O.S. Urgut, C.N. Banti, N. Kourkoumelis, A.M. Owczarzak, M. Kubicki, K. Charalabopoulos, S.K. Hadjikakou, Polyhedron 52 (2013) 1403-1410

[21] I.I. Ozturk, S.K. Hadjikakou, N. Hadjiliadis, N. Kourkoumelis, M. Kubicki, M. Baril, I.S. Butler, J. Balzarini, Inorg Chem 46 (2007) 8652-8661

[22] I.I. Ozturk, S.K. Hadjikakou, N. Hadjiliadis, N. Kourkoumelis, M. Kubicki, A.J. Tasiopoulos, H. Scleiman, M.M. Barsan, I.S. Butler, J. Balzarini, Inorg Chem 48 (2009) 2233-2245

[23] I.I. Ozturk, S. Filimonova, S.K. Hadjikakou, N. Kourkoumelis, V. Dokorou, M.J. Manos, A.J. Tasiopoulos, M.M. Barsan, I.S. Butler, E.R. Milaeva, J. Balzarini, N. Hadjiliadis, Inorg Chem 49 (2010) 488-501

[24] D.J.A. de Groot, E.G.E. de Vries, H.J.M. Groen, S. de Jong, Crit Rev Oncol Hemat 61 (2007) 52-69

[25] S.J. Baek, T.E. Eling, Prog Lipid Res 45 (2006) 1-16

[26] E.S. Schernhammer, J.H. Kang, A.T. Chan, D.S. Michaud, H.G. Skinner, E. Giovannucci, G.A. Colditz, C.S. Fuchs, J Natl Cancer I 96 (2004) 22-28

[27] R.E. Harris, R.T. Chlebowski, R.D. Jackson, D.J. Frid, J.L. Ascenseo, G. Anderson, A. Loar, R.J. Rodabough, E. White, A. McTiernan, Cancer Res 63 (2003) 6096-6101

[28] R.A. Gupta, R.N. DuBois, Nat Rev Cancer 1 (2001) 11-21

[29] A. Catalano, A. Procopio, Histol Histopathol 20 (2005) 969-975.

[30] G.A. Piazza, A.K. Rahm, T.S. Finn, B.H. Fryer, H. Li, A.L. Stoumen, R. Pamukcu, D.J. Ahnen, Cancer Res 57 (1997) 2452-2459

[31] D.J.E. Elder, D.E. Halton, A. Hague, C. Paraskeva, Clin Cancer Res 3 (1997) 1679-1683

[32] R. Hanif, A. Pittas, Y. Feng, M.I. Koutsos, L. Qiao, L. StaianoCoico, S.I. Shiff, B. Rigas, Biochem Pharmacol 52 (1996) 237-245

[33] V.P. Torchilin, J Control Release 73 (2001) 137-172

[34] M.A. Zoroddu, S. Medici, A. Ledda, V.M. Nurchi, J.I. Lachowicz, M. Peana, Curr. Med. Chem. 21 (2014) 3837-3853

[35] S. Eckhardt, P.S. Brunetto, J. Gagnon, M. Priebe, B. Giese, K.M. Fromm Chem. Rev., 113 (2013) 4708-4754

[36] A.S. Narang, D. Delmarre, D. Gao, Int J Pharm 345 (2007) 9-25.

[37] E.C. Dreaden, A.M. Alkilany, X.H. Huang, C.J. Murphy, M. El-Sayed, Chem Soc Rev 41 (2012) 2740-2779.

[38] R. Fenger, E. Fertitta, H. Kirmse, A.F. Thunemann, K. Rademann, Phys Chem Chem Phys 14 (2012) 9343-9349

[39] Y.F. Wang, D.S.D. Larsson, D. van der Spoel, Biochemistry-Us 48 (2009) 1006-1015

[40] B. Isomaa, J. Reuter, B.M. Djupsund, Arch Toxicol 35 (1976) 91-96

[41] E. Ito, K.W. Yip, D. Katz, S.B. Fonseca, D.W. Hedley, S. Chow, G.W. Xu, T.E. Wood, C. Bastianutto, A.D. Schimmer, S.O. Kelley, F.F. Liu, Mol Pharmacol 76 (2009) 969-983

[42] Effendy, J.D. Kildea, A.H. White, Aust J Chem 50 (1997) 671-674

[43] G. Smith, C.H.L. Kennard, T.C.W. Mak, Z Kristallogr 184 (1988) 275-280

[44] M.I. Azocar, G. Gomez, P. Levin, M. Paez, H. Munoz, N. Dinamarca, J Coord Chem 67 (2014) 3840-3853

[45] M.A. Abdellah, S.K. Hadjikakou, N. Hadjiliadis, M. Kubicki, T. Bakas, N. Kourkoumelis, Y.V. Simos, S. Karkabounas, M.M. Barsan, I.S. Butler, Bioinorg Chem Appl 2009, 542979, doi: 10.1155/2009/542979.

[46] D.L. Baun, T. H. Christensen, Waste Manage Res 22 (2004) 3-23.

[47] D.L. Perry, S.L. Phillips, Handbook of Inorganic Compounds, Taylor & Francis Inc., 1995

[48] H.S. Katz, Handbook of Fillers for Plastics, Kluwer Academic Publishers Group 1987

[49] L. Wang, H. Chen, Y.-e. He, Y. Li, M. Li, X. Li, Appl Catal A 242 (2003) 85-88.

[50] C.-Y. Zhou, J. Zhao, Y.-B. Wu, C.-X. Yin, Y. Pin, J Inorg Biochem 101 (2007) 10-18

[51] M.H. Hanigan, P. Devarajan, Cancer Ther., 1 (2003) 47-61

[52] CRYSALIS RED, version 1.171.31.5; Oxford Diffraction Ltd. (release 28-08-2006 CRYSALIS 171.NET).

[53] Oxford Diffraction, CRYSALIS CCD and CRYSALIS RED, version p171.29.2; Oxford Diffraction Ltd., Abingdon, Oxford, England, 2006.

[54] G.M. Sheldrick, Acta Crystallogr A 46 (1990) 467-473.

[55] G.M. Sheldrick, Acta Crystallogr A 64 (2008) 112-122.

Table 1: Atomic absorption analysis results

Micelle	m_{tot} (μg)	m_{Ag} (μg)	Percentage (%)
a	11600	6.77	0.66
b	9360	4.65	0.60
c	54170	76.3	1.76

Where, m_{tot}, the total mass of the micelle that was analysed,
m_{Ag}, the detected mass of silver in the sample and
Percentage (%), the percentage of the compound in the respective micelle.

Table 2: IC_{50} values for cell viability found for complexes **1**–**3** and their micelles **a**–**c** against MCF-7 (breast, ER positive), MDA-MB-231 (breast, ER negative) and the normal human lung cell line MRC-5 (normal human fetal lung fibroblast cells).

Compound	IC_{50} (μM)					
	MCF-7	MDA-MB-231	MRC-5	TPI MCF-7	TPI MDA-MB-231	Ref.
$Ag(Ph_3Sb)_3(NO_3)$ (**1**)	3.05±0.11	5.67±0.17	4.36±0.44	1.42	0.77	
Micelle **a**	0.045±0.004	0.042±0.002	0.070±0.008	1.56	1.66	
$Ag(Ph_3Sb)_3$(SalH) (**2**)	3.19±0.07	7.26±0.18	5.03±0.12	1.58	0.69	
Micelle **b**	0.048±0.006	0.044±0.004	0.062±0.005	1.29	1.41	
$Ag(Ph_3Sb)_3$(Asp) (**3**)	5.88±0.39	14.86±0.86	4.75±0.82	0.81	0.32	
Micelle **c**	0.103±0.011	0.157±0.013	0.263±0.050	2.55	1.67	
$[Ag(tpp)_2(salH)]$	2.3±0.3	-	3.1±0.3	1.35	-	[16]
$\{[Ag(tpp)_3(asp)](dmf)\}$	2.3±0.3	-	2.9±0.1	1.26	-	[16]
$[Ag(tptp)_2(salH)]$	1.7±0.3	-	-		-	[11]
$[Ag(tmtp)_2(salH)]$	5.9±0.8	-	-		-	[11]

Table 3. Bioactivity data recorded for micelles **a-c** and silver(I) complexes with anti-inflammatory drugs or agents and arylphosphines.

Complexes	K_b (M^{-1}) $(\times 10^4)$	K_{app} (M^{-1}) $(\times 10^4)$	IC_{50} (μM) *LOX*	*Ref.*
Micelle **a**	3.3±0.1	2239±178	8.4	*
Micelle **b**	10.0±0.1	2261±133	29.4	*
Micelle **c**	2.5±0.1	1128±250	>30	*
$[Ag(tptp)_2(salH)]$	7.2±1.1	0.6±0.2	>30	[16]
$\{[Ag(tpp)_3(asp)](dmf)\}$	11.0±2.8	-	7.2	[16]
$[Ag(tpp)_2(salH)]$	13.3±6.5	-	2.3	[11]
$[Ag(tmtp)_2(salH)]$	5.3±0.8	1.7±0.1	>30	[11]

* this work

Table 4: Initial rates of the reactions between **b-c** and **GSH** obtained from UV absorption data at 280 nm as a function of time (0 to 300 min). The differences were fitted to the equation: $I_d = C + A_1 \exp(-b_1 t) + A_2 \exp(-b_2 t)$, while the initial slope (Sin) was calculated as $-(A_1 b_1 + A_2 b_2)$.

Compound	**Concentration (µM)**	**Glutathione (mM)**	**Initial Slope (min^{-1})**	**R^2**
a	150	16.5	0.0057	0.89
	310	16.5	0.0108	0.87
	580	16.5	0.0284	0.96
b	360	16.5	0.0011	0.94
	730	16.5	0.0016	0.94
	1360	16.5	0.0030	0.99

Figure Captions

Figure 1 Molecular diagrams of the ligands used.

Figure 2 The structure of the asymmetric unit of the compound [$Ph_3Sb(Ac)_2$] and its molecular packing scheme along b axis. Selected bond lengths (Å) and angles [^{o}]: Sb1-O1= 2.128(4), Sb1-C1= 2.112(5), Sb1-C7= 2.116(7), O1-C11= 1.303(7), O2-C11= 1.222(7), O1-Sb1-C1 = 89.79(18), O1-Sb1-C7 = 87.62(11), O1-Sb1-O1_a= 175.24(15), O1-Sb1-C1_a= 91.53(18), C1-Sb1-C7= 106.10(16), O1_a-Sb1-C1= 91.53(18), C1 -Sb1-C1= 147.8(2), O1_a-Sb1-C7= 87.62(11), C1_a-Sb1-C7= 106.10(16), O1_a-Sb1-C1= 89.79(18)

Figure 2 The structure of the asymmetric unit of compound **2**. Phenyl protons are omitted for clarity. The dashed line represents the intramolecular hydrogen bond. Selected bond lengths (Å) and angles [^{o}]: Ag-O(1)= 2.305(6), Ag-Sb(2)= 2.6955(7), Ag-Sb(1)= 2.7161(7), Ag-Sb(3)= 2.7994(8), O(1)-C(1)= 1.151(11), O(2)-C(1)= 1.295(12), O(3)-C(7)= 1.278(10), O(3)-H(100)= 1.02(2), O(1)-Ag-Sb(2)= 121.41(16), O(1)-Ag-Sb(1)= 118.22(18), Sb(2)-Ag-Sb(1)= 113.51(2), O(1)-Ag-Sb(3)= 78.3(2), Sb(2)-Ag-Sb(3)= 109.05(2), Sb(1)-Ag-Sb(3)= 109.10(2)

Figure 4 The structure of the asymmetric unit of compound **3**. Phenyl protons are omitted for clarity. Selected bond lengths (Å) and angles [^{o}]: Sb(1)-Ag= 2.7232(7), Sb(2)-Ag= 2.7394(7), Sb(3)-Ag= 2.7179(8), Ag-O(1) = 2.391(5), O(1)-C(1)= 1.250(9), O(2)-C(1)= 1.247(8), O(3)-C(8)= 1.335(10), O(3)-C(7)= 1.399(9), O(4)-C(8)= 1.209(10), O(1)-Ag-Sb(3)= 103.17(13), O(1)-Ag-Sb(1)= 103.72(13), Sb(3)-Ag-Sb(1)= 125.25(2), O(1)-Ag-Sb(2)= 90.75(12), Sb(3)-Ag-Sb(2)= 116.88(2), Sb(1)-Ag-Sb(2)= 109.48(2)

Figure 5 XRF analysis asserts the encapsulation of the complexes in the micelles. The calculated Sb:Ag ratio in micelles **a-c** are 2.03 ± 0.22 (**a**) 2.24 ± 0.24 (**b**) and 2.24 ± 0.24 (**c**)

Figure 6 CMC determination for the surfactant CTAB via conductivity in presence of (a) only aqua medium, (b) 1:1 CH_3CH_2OH/ CH_3CH_2CN, 3 mL (co-solvents), (c) co-solvents and compound **1** (C= 5 x 10^{-3} M), (d) co-solvents and compound **2** (C= 5 x 10^{-3} M) and (e) co-solvents and compound **3** (C= 5 x 10^{-3} M).

Figure 7 Emission spectrum of EB bound to DNA (peak around 610 nm) decreases in order of the concentration of the complex as indicated at the bottom of each of the three panels from left to right. Inset shows the plots of emission intensity *I*o/*I vs.* [complex].

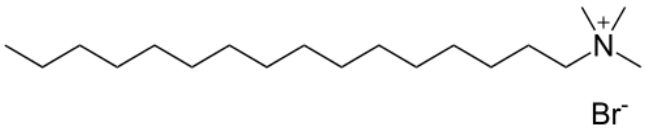

CTAB

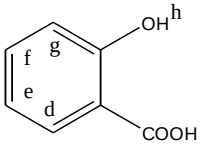

$SalH_2$

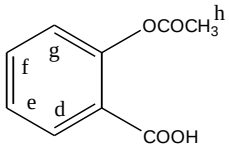

AspH

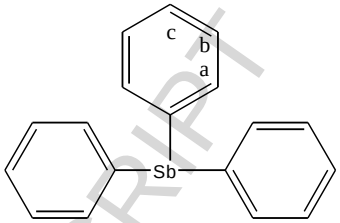

Ph_3Sb

Figure 1

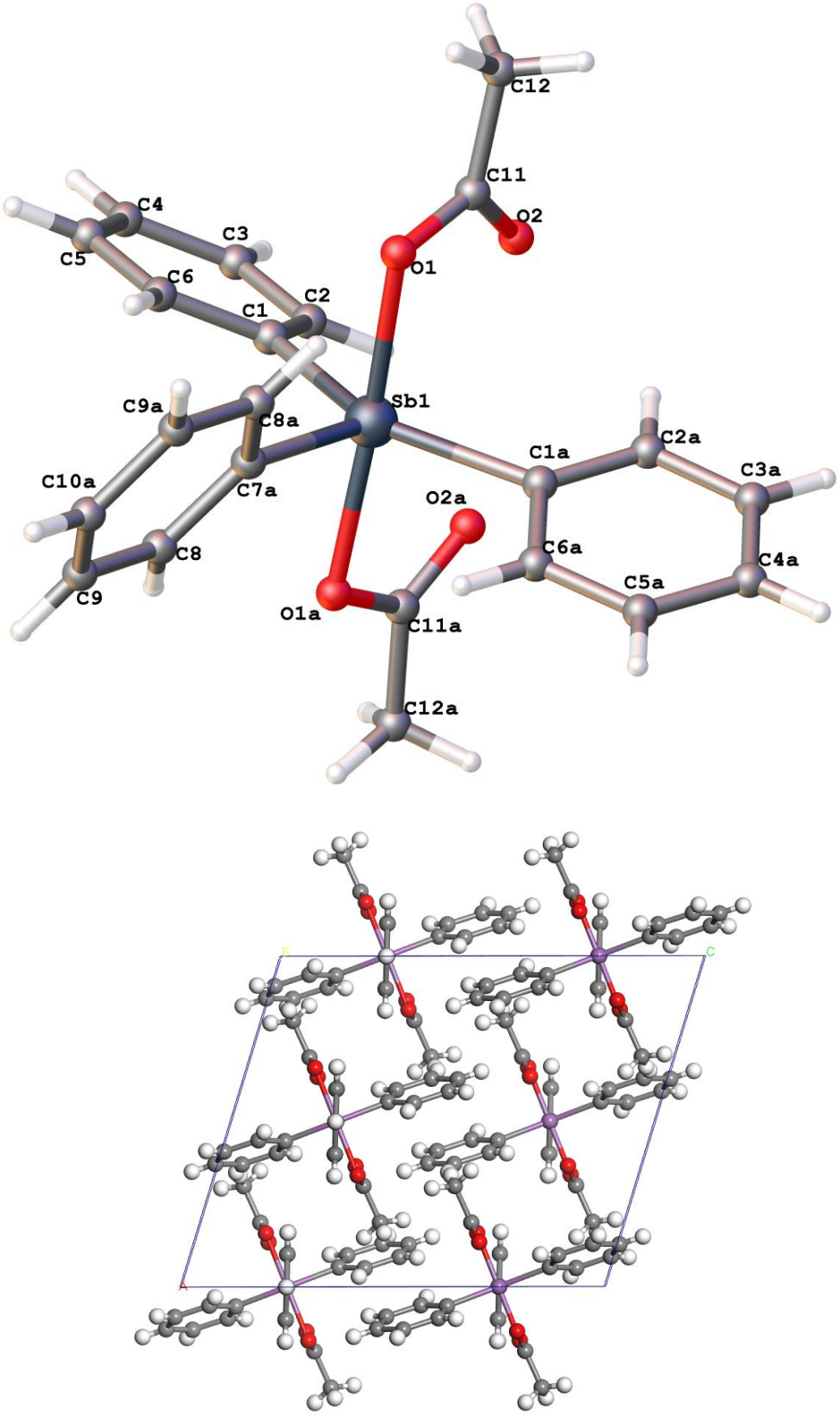

Figure 2

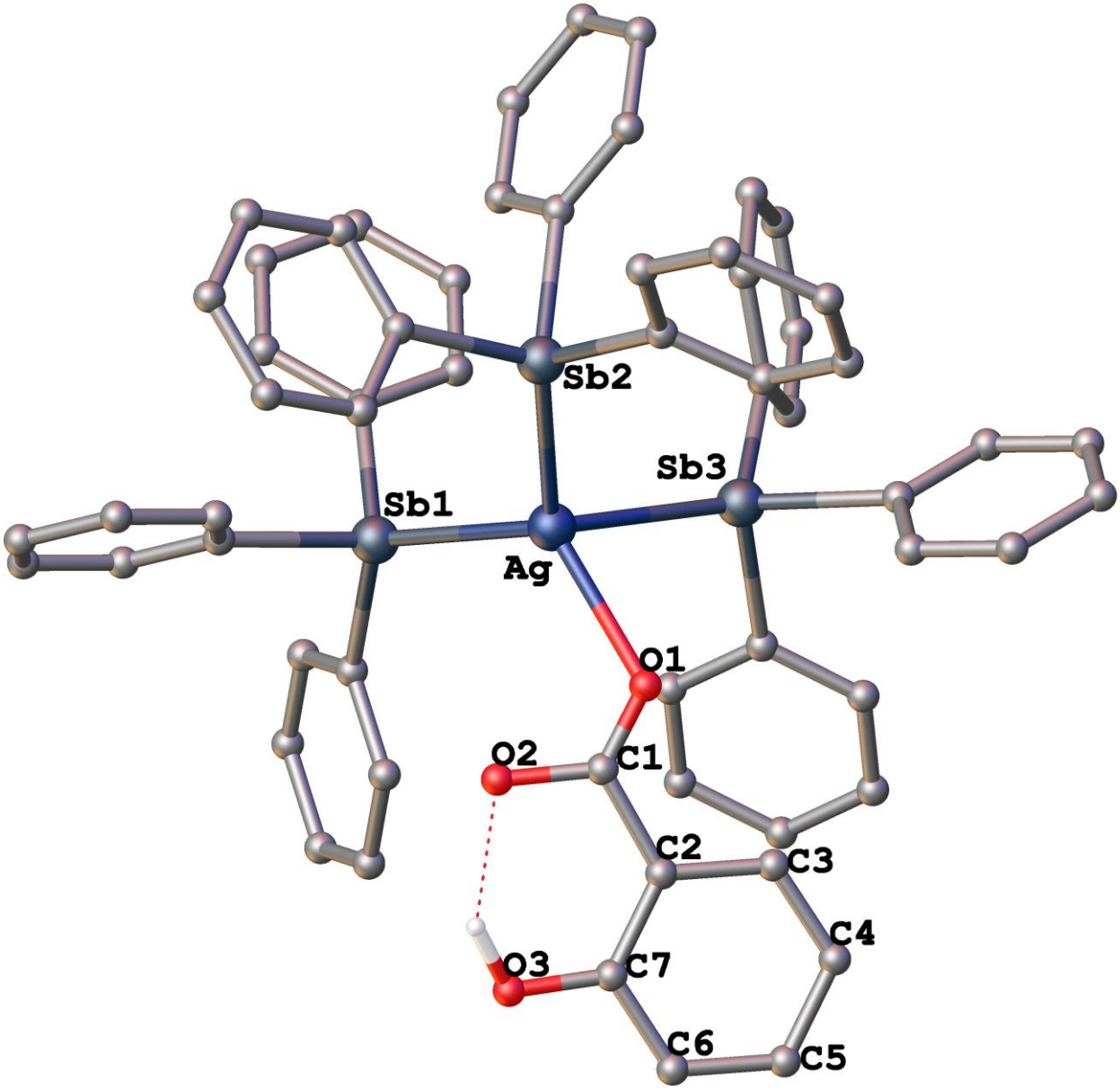

Figure 3

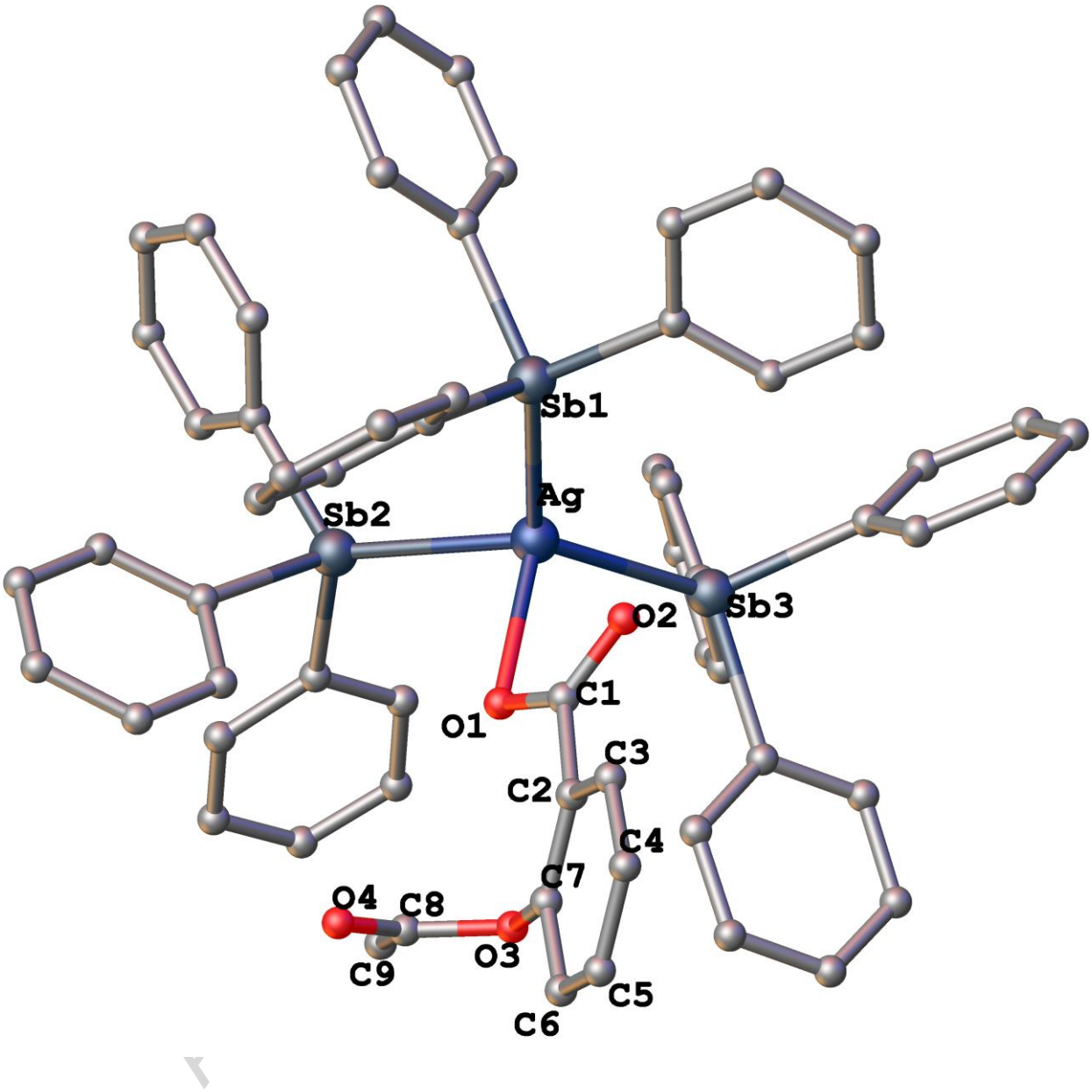

Figure 4

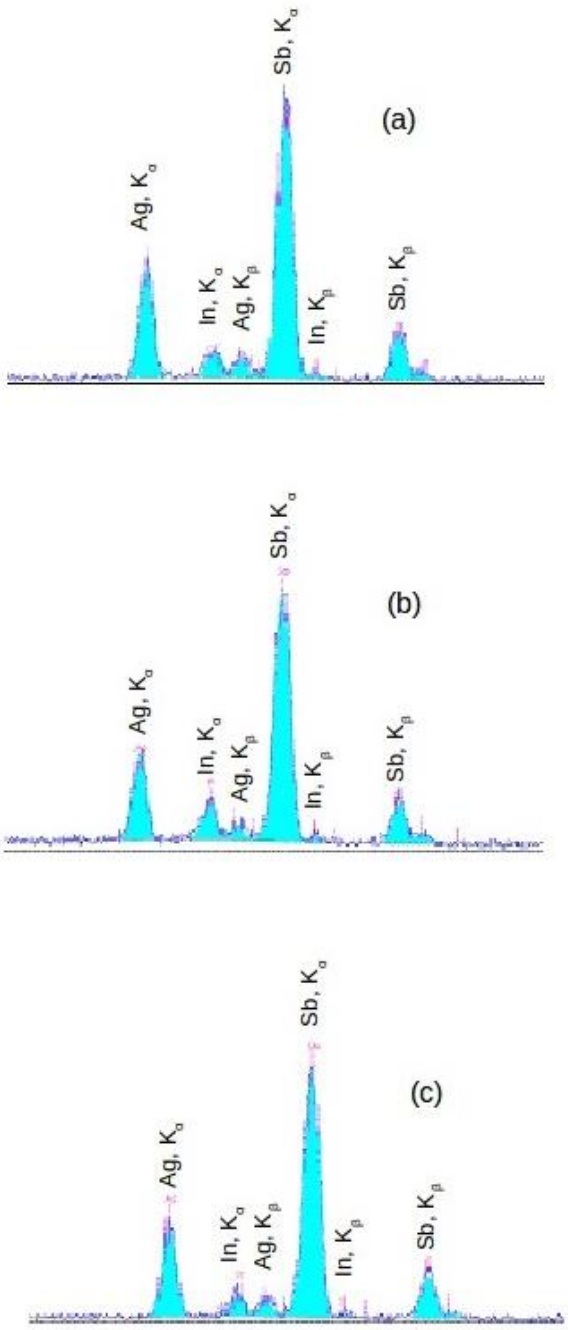

Figure 5

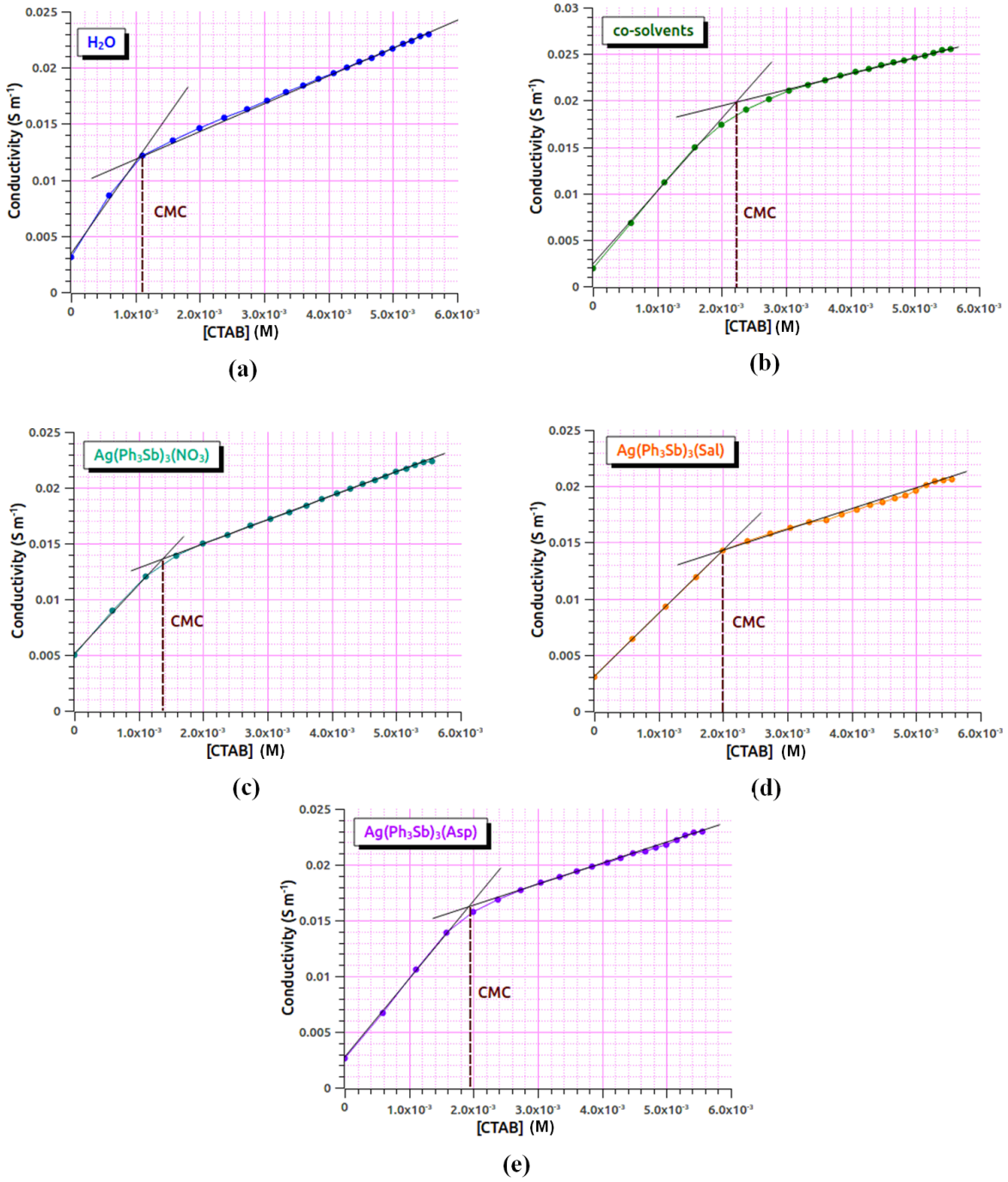

Figure 6

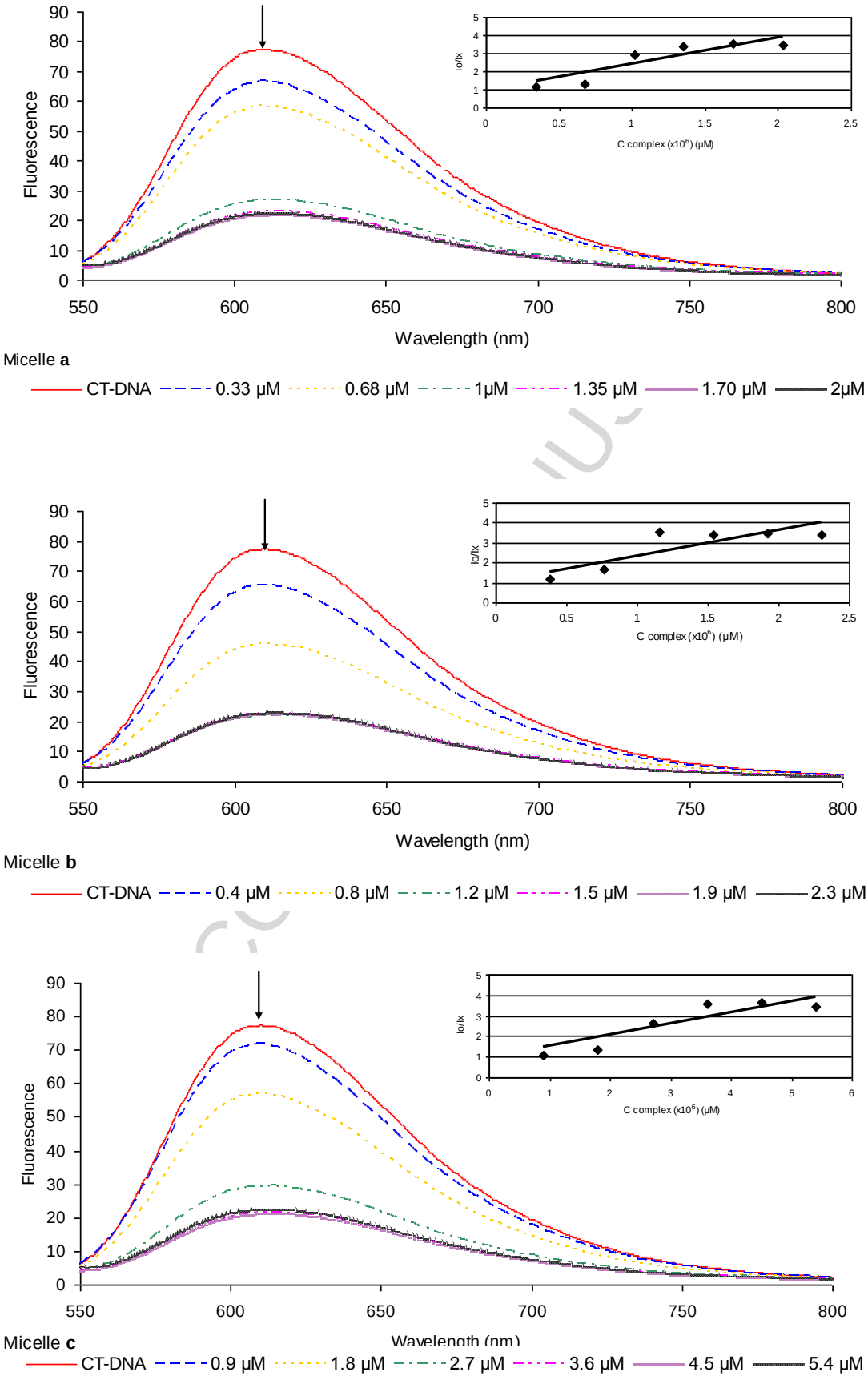
Fluorescence
Wavelength (nm)
Io/Ix
C complex (x10⁶) (μM)
Micelle a
CT-DNA
0.33 μM
0.68 μM
1μM
1.35 μM
1.70 μM
2μM
Micelle b
CT-DNA
0.4 μM
0.8 μM
1.2 μM
1.5 μM
1.9 μM
2.3 μM
Micelle c
CT-DNA
0.9 μM
1.8 μM
2.7 μM
3.6 μM
4.5 μM
5.4 μM

Figure 7

Synopsis for Graphical Abstract

The mixed metal Ag(I)-Sb(III) compounds of formula $\{Ag(Ph_3Sb)_3(NO_3)\}$(**1**), $\{Ag(Ph_3Sb)_3(SalH)]\}$(**2**) and $\{Ag(Ph_3Sb)_3(Asp)\}$(**3**) have been synthesised and characterised. Compounds and their micelles with CTAB were evaluated for their *in vitro* cytotoxicity against the MCF-7, MDA-MB-231 and MRC-5 cells. The micelles show significant higher activity than that of the initial compounds.

Pictogram for Graphical Abstract

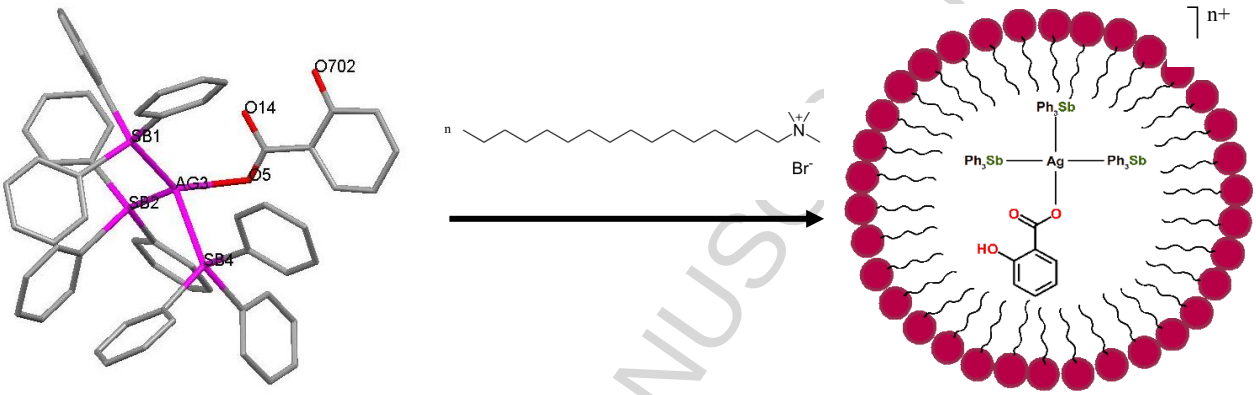

Research Highlights

- New Metallotherapeutic compounds of NSAIDs.
- Micelles with enhanced solubility.
- Cytostatic activity of the complex.
- Binding affinity towards CT-DNA, lipoxygenase (LOX) and glutathione (GSH)